Uniform saturation of a strongly coupled spin system by two-frequency irradiation

Jae-Seung Lee,[1,2] Anatoly K. Khitrin,[3] Ravinder R. Regatte,[2] and Alexej Jerschow[1,a)]
[1]*Department of Chemistry, New York University, New York, New York 10003, USA*
[2]*Quantitative Multinuclear Musculoskeletal Imaging Group, Center for Biomedical Imaging, Department of Radiology, New York University Langone Medical Center, New York, New York 10016, USA*
[3]*Department of Chemistry, Kent State University, Kent, Ohio 44242, USA*

(Received 4 April 2011; accepted 26 May 2011; published online 16 June 2011)

The theoretical basis of two-frequency saturation is given here in the framework of Provotorov theory. The parameters influencing the saturation efficiency are discussed and studied experimentally using a liquid-crystalline test system. It is shown that double-frequency irradiation can be extremely efficient when the irradiation frequencies are placed at opposite sides of the characteristic frequency of the spin system, and that the frequency separation in the double-frequency irradiation can be varied over a large range. Provotorov theory is also shown to provide good insights into the experimental findings, which would otherwise be difficult to obtain from simulations. © *2011 American Institute of Physics*. [doi:10.1063/1.3600758]

I. INTRODUCTION

Saturation is one of the central phenomena extensively studied in the field of nuclear magnetic resonance (NMR). For a system of non-interacting spins 1/2, long rf irradiation decreases the population difference between the spin up and down states from its thermal equilibrium value. The system eventually reaches a steady state manifesting a balance between the driving forces of the external rf irradiation decreasing the population difference and the relaxation mechanisms recovering the population difference in the thermal equilibrium state.[1] For a system of strongly coupled spins 1/2, continuous rf irradiation brings the system into an internal equilibrium between the Zeeman and dipolar reservoirs, which is well understood in terms of the concept of spin temperature.[2–4] Usually, the rf irradiation for saturation is assumed to consist of only one frequency component. Continuous NMR methodology depends on monitoring the magnetization while varying the frequency of the saturating rf irradiation, which reveals information about the spectral lineshape.

Among the contemporary applications of saturation, chemical exchange saturation transfer (CEST) and magnetization transfer (MT) are emerging as important magnetic resonance imaging (MRI) contrast mechanisms.[5,6] In these methods, rf irradiation off-resonant to water protons is applied to saturate protons belonging to targeted small or macromolecules, and the change in the magnetization of water protons is monitored to indirectly detect such molecules. Since MT and CEST together with direct water proton saturation can happen simultaneously in tissues, it is important to discriminate among different saturation effects in order to obtain more quantitative information about the targeted molecules.

Liquid crystal and other oriented media have been used to study many molecular structures by introducing residual dipolar couplings.[7,8] When a liquid crystal is used as a host, its broad proton NMR spectrum appears together with the narrower and sharper spectral lines from a guest molecule and it is often desirable to eliminate the broad spectral components. A common solution is the delayed acquisition, to eliminate the short-lived component from the liquid crystal and to collect only the signal from a guest molecule in the free induction decay. This approach, however, often causes distortion of the baseline, which may not be easily corrected in the resultant NMR spectrum due to the evolution under the internal Hamiltonian during the acquisition delay. Therefore, a clean saturation of the NMR spectrum of the host liquid crystal is desirable in practice.

It has been shown that uniform and efficient saturation in strongly coupled spin systems can be achieved by using two-frequency rf irradiation.[9] This approach can be extremely useful for CEST contrast in imaging, when one desires to separate MT effects from CEST effects, or for eliminating the signal from the liquid-crystalline solvent.[9] Here we present a detailed analysis, based on Provotorov theory, as well as experiments on a liquid-crystalline system, in order to study the parameters influencing the performance of the two-frequency irradiation technique.

II. THEORY

Provotorov's thermodynamic theory has been used to describe the dynamics of a strongly coupled spin system under a weak rf irradiation.[3,10] By treating the weak rf irradiation as a perturbation, the master equation can be solved by iteration under the assumption that the density operator is described at all times by a quasi-equilibrium form $\rho(t) = (1/2^N)[1 + \beta_S(t)\omega_0 S_z - \beta_d(t)\mathcal{H}_d]$, where β_S and β_d are, respectively, the Zeeman and dipolar inverse spin temperatures, ω_0 is the resonance frequency, and $\mathcal{H}_d$ is the dipole-dipole interaction Hamiltonian. Traditionally, a set of first-order

a)Author to whom correspondance should be addressed. Electronic mail: alexej.jerschow@nyu.edu.

coupled differential equations can be derived for the inverse spin temperatures β_S and β_d. Instead, by introducing the spin and dipolar polarizations $P_S = (2/N)\langle S_z\rangle$ and $P_d = (2/N)(\langle \mathcal{H}_d\rangle/\omega_{\rm loc})$, one can obtain a set of kinetic equations as follows:[11]

$$\frac{dP_S}{dt} = -W\left(P_S - \frac{\Delta}{\omega_{\rm loc}}P_d\right), \tag{1}$$

$$\frac{dP_d}{dt} = W\frac{\Delta}{\omega_{\rm loc}}\left(P_S - \frac{\Delta}{\omega_{\rm loc}}P_d\right), \tag{2}$$

where $\langle O\rangle \equiv \mathrm{tr}\{O\rho\}$, $\omega_{\rm loc} \equiv \mathrm{tr}\{\mathcal{H}_d^2\}/\mathrm{tr}\{S_z^2\}$, $\Delta \equiv \omega_0 - \omega$ is the frequency difference between the resonance frequency ω_0 and the frequency ω of the weak rf irradiation, $W = \pi\omega_1^2 g(\Delta)$, ω_1 is the amplitude of the weak rf irradiation, and $g(\Delta)$ is the normalized absorption line shape.

It is straightforward to incorporate another weak rf irradiation at the frequency ω' into the above equation. Each frequency contributes to kinetics in the same way as in Eqs. (1) and (2), and the cross effect, which depends on the time integral $\int\int dt'dt'' \cos\omega t' \cos\omega' t''$, will be negligible unless the two frequencies are so close that the difference between them is comparable to the amplitude of the rf fields. Therefore, with two weak rf irradiations, the kinetic equations will read,

$$\frac{dP_S}{dt} = -W\left(P_S - \frac{\Delta}{\omega_{\rm loc}}P_d\right) - W'\left(P_S - \frac{\Delta'}{\omega_{\rm loc}}P_d\right), \tag{3}$$

$$\frac{dP_d}{dt} = W\frac{\Delta}{\omega_{\rm loc}}\left(P_S - \frac{\Delta}{\omega_{\rm loc}}P_d\right) + W'\frac{\Delta'}{\omega_{\rm loc}}\left(P_S - \frac{\Delta'}{\omega_{\rm loc}}P_d\right), \tag{4}$$

where the primed symbols W' and Δ' are the transition rate and the offset for the irradiation at ω'.

From Eqs. (3) and (4), one can obtain two eigenvalues governing the dynamics,

$$\lambda_\pm = -\frac{1}{2}\left\{\left(W + W' + \frac{W\Delta^2 + W'\Delta'^2}{\omega_{\rm loc}^2}\right) \pm \sqrt{\left(W + W' - \frac{W\Delta^2 + W'\Delta'^2}{\omega_{\rm loc}^2}\right)^2 + \frac{4(W\Delta + W'\Delta')^2}{\omega_{\rm loc}^2}}\right\}, \tag{5}$$

which are always real and negative. Since the solutions for $P_S(t)$ and $P_d(t)$ have the form of $A\exp(\lambda_+ t) + B\exp(\lambda_- t)$, with the constants A and B set according to the initial states, $P_S(\infty) = P_d(\infty) = 0$, which means that the spin and dipolar polarizations vanish under two-frequency rf irradiation.

In the presence of spin-lattice relaxation, the spin and dipolar polarizations do not decay to zero, but reach steady states. This can be easily taken into account by adding the terms $-(P_S - P_0)/T_1$ and $-P_d/T_d$ to Eqs. (3) and (4), respectively,

$$\frac{dP_S}{dt} = -W\left(P_S - \frac{\Delta}{\omega_{\rm loc}}P_d\right) - W'\left(P_S - \frac{\Delta'}{\omega_{\rm loc}}P_d\right) - \frac{P_S - P_0}{T_1}, \tag{6}$$

$$\frac{dP_d}{dt} = W\frac{\Delta}{\omega_{\rm loc}}\left(P_S - \frac{\Delta}{\omega_{\rm loc}}P_d\right) + W'\frac{\Delta'}{\omega_{\rm loc}}\left(P_S - \frac{\Delta'}{\omega_{\rm loc}}P_d\right) - \frac{P_d}{T_d}, \tag{7}$$

where T_1 and T_d are the spin-lattice relaxation times for the Zeeman and dipolar reservoirs, respectively, and P_0 is the thermal equilibrium polarization. For the inhomogeneous equations Eqs. (6) and (7), $P_S(t)$ and $P_d(t)$ have the form of $A\exp(\lambda_+ t) + B\exp(\lambda_- t) + C$, where $C \neq 0$. By replacing dP_S/dt and dP_d/dt with zero, one can obtain the steady-state polarizations as

$$P_S(\infty) = P_0\frac{\omega_{\rm loc}^2 + T_d(W\Delta^2 + W'\Delta'^2)}{\omega_{\rm loc}^2 + \omega_{\rm loc}^2 T_1(W + W') + T_d(W\Delta^2 + W'\Delta'^2) + T_1T_dWW'(\Delta - \Delta')^2}, \tag{8}$$

$$P_d(\infty) = P_0\frac{\omega_{\rm loc}T_d(W\Delta + W'\Delta')}{\omega_{\rm loc}^2 + \omega_{\rm loc}^2 T_1(W + W') + T_d(W\Delta^2 + W'\Delta'^2) + T_1T_dWW'(\Delta - \Delta')^2}. \tag{9}$$

And the two eigenvalues $\lambda_\pm$,

$$\lambda_\pm = -\frac{1}{2}\left\{\left(\frac{1}{T_1} + \frac{1}{T_d} + W + W' + \frac{W\Delta^2 + W'\Delta'^2}{\omega_{\rm loc}^2}\right) \pm \sqrt{\left(\frac{1}{T_1} - \frac{1}{T_d} + W + W' - \frac{W\Delta^2 + W'\Delta'^2}{\omega_{\rm loc}^2}\right)^2 + \frac{4(W\Delta + W'\Delta')^2}{\omega_{\rm loc}^2}}\right\}, \tag{10}$$

are still real and negative.

III. RESULTS

The kinetic equations introduced in Sec. II predict that the time evolution of the spin and dipolar polarizations are bi-exponential. Since the initial state is always the thermal equilibrium state, the spin polarization would decay monotonously from its maximum value to the smaller final value, in which case it may be hard to see whether its time evolution is bi-exponential or not. Instead, the dipolar polarization is initially zero, so its evolution is expected to clearly reveal the bi-exponential time behavior in the form of buildup and subsequent decay.

In this study, liquid crystal 5CB was chosen for numerical and experimental tests. The proton NMR experiments have been performed using a Bruker Avance 500 MHz NMR spectrometer. The proton NMR spectrum was obtained by applying a 9.5 μs 90° pulse to the thermal equilibrium state (Fig. 1(a)). The spin-lattice relaxation time for the Zeeman reservoir T_1 was measured with the inversion recovery sequence, and the spin-lattice relaxation time for the dipolar reservoir T_d was measured with adiabatic demagnetization in the rotating frame (ADRF) followed by adiabatic remagnetization in the rotating frame (ARRF) after variable delays. The ADRF and ARRF were performed by 1 ms-long linear decreasing and increasing ramps, respectively. Before the ADRF, the spin polarization was brought to the transverse plane by the 90° pulse. Mono-exponential fitting was applied to the experimental data to estimate the spin-lattice relaxation times to be $T_1 = 1.0$ s and $T_d = 0.4$ s.

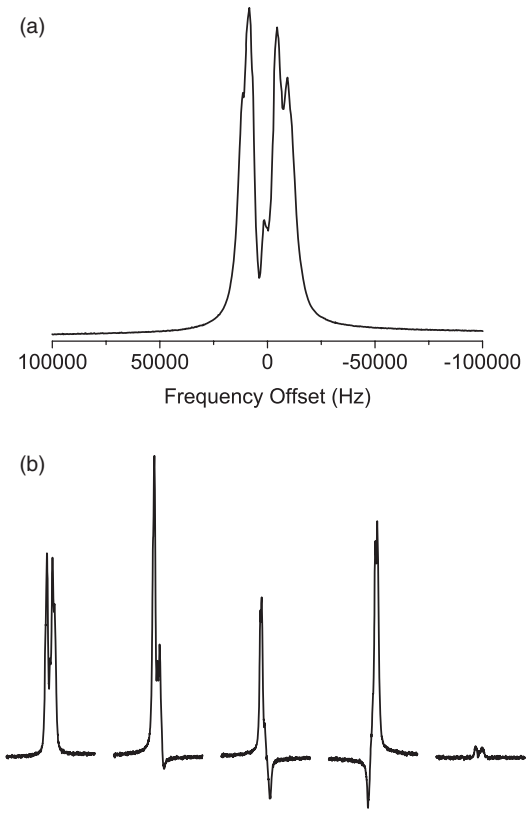

FIG. 1. (a) Proton NMR spectrum of 5CB with a 9.5 μs 90° pulse on the thermal equilibrium state. (b) Linear-response spectra of 5CB with a 5° reading pulse on (leftmost) the thermal equilibrium state, (second to fourth) the states after 50 ms-long rf irradiation at the frequency offsets of −8 kHz, 0 kHz, and +8 kHz with rf amplitude of 500 Hz, and (rightmost) the state after a 50ms-long on-resonant cosine pulse with a modulation frequency of 8 kHz and rf amplitude of 1 kHz.

The effect of two-frequency saturation is briefly depicted in Fig. 1(b). Five linear-response spectra were obtained by applying a 5° reading pulse to the thermal equilibrium state, the states after rf irradiation at the frequency offsets of −8 kHz, 0 kHz, and +8 kHz, and the state after a on-resonant cosine pulse with the modulation frequency of 8 kHz. A linear-response spectrum with a small-angle reading pulse reveals the population differences between the energy levels of a given spin state. The duration of the single-frequency rf irradiation and the cosine pulse was 50 ms and the rf amplitudes $\gamma B_1/2\pi$ were, respectively, 500 Hz and 1 kHz, so that the individual frequency components of the cosine pulse have the same rf amplitude as the single-frequency pulse. The linear-response spectrum after the cosine pulse presents peaks with very small intensity, which suggests that the system is approaching the state with equal populations across all the energy levels. On the other hand, the linear-response spectra after single-frequency rf irradiation give rise to positive and negative peaks, which means that there exists a nonuniform population distribution in the spin system.

The proton NMR spectrum and relaxation times were used to numerically solve Eqs. (6) and (7). The numerical solutions for $P_S(t)$ and $P_d(t)$ were obtained by using the ode45 function in MATLAB. The amplitude of the rf irradiation $\omega_1/2\pi$ and dipolar local field $\omega_{\text{loc}}/2\pi$ were set to 500 Hz and 10 kHz, respectively. (From the integrated proton NMR spectrum, $\omega_{\text{loc}} \sim 2\pi \times 6$ kHz.) As seen in Figs. 2(a) and 2(b), P_S and P_d are zero for a large range of the frequency combinations only 50 ms after the two-frequency irradiations starts.

In the experiments, two-frequency irradiation was implemented by cosine shaped pulses. A cosine pulse with a modulation frequency of f Hz provides rf irradiation at $\pm f$ Hz. Then, by shifting the center of the cosine pulse, a range of frequency combinations can be sampled. We prepared 50 ms-long cosine pulses with the modulation frequencies from 0 Hz to 20 kHz with increments of 1 kHz and swept their center frequencies from −30 kHz to 30 kHz with increments of 2 kHz. The rf amplitudes of the pulses were set to 1 kHz, so each frequency component has an rf amplitude of 500 Hz. At the end of the cosine pulse, the 90° hard pulse or the ARRF sequence were applied to measure P_S or P_d. Since P_S and P_d are longitudinal, a simple four-step phase cycling was applied to remove any residual transverse components of the magnetization that may appear after the cosine pulses. The results are shown in Figs. 2(c) and 2(d) for two irradiation frequencies varying independently between −20 kHz and 20 kHz.

The experimental results look similar to the numerical solutions. The Zeeman polarization P_S (Figs. 2(c)) turns to zero for a large range of frequencies, especially when one frequency is positive and the other is negative or when the rf irradiation is applied at frequencies where the spectral intensity is large. Small residual dipolar polarization P_d (Fig. 2(d)) in the region where P_S is zero is uniform. We should note that the possibilities of using a direct numerical simulation of spin dynamics to reproduce the results in

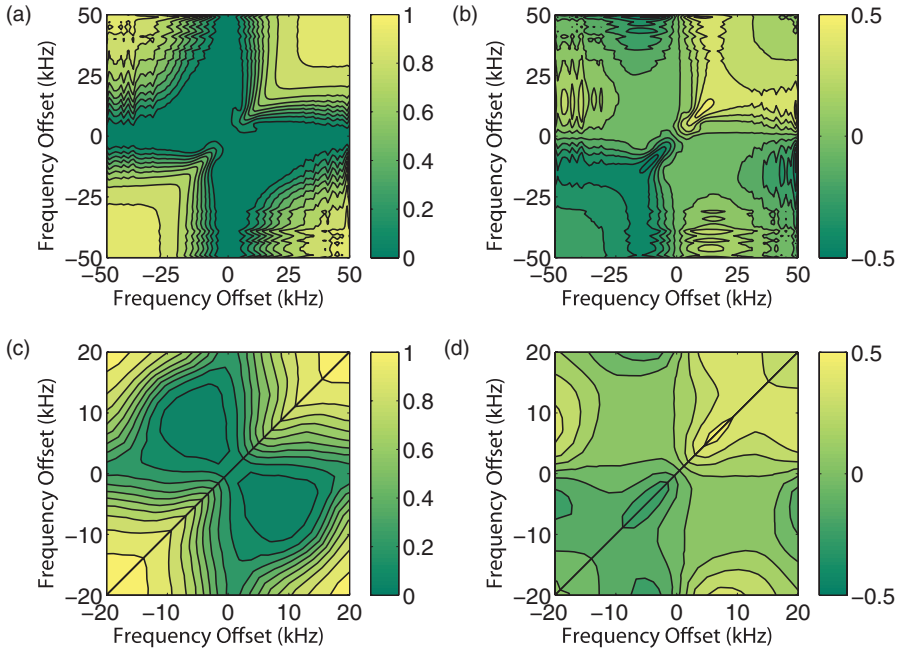

FIG. 2. (a) Zeeman and (b) dipolar orders calculated by solving the dynamic equations. (c) Zeeman and (d) dipolar orders experimentally measured in 5CB. The two-frequency irradiations are 50 ms-long cosine-modulated pulses with an rf amplitude $\gamma B_1/2\pi = 1$ kHz.

Fig. 2 are very limited. For time-independent Hamiltonians, such simulations can be performed on spin systems of up to 12–13 spins (and slightly larger using symmetry arguments). This number of spins is not enough to describe the behavior in the thermodynamic limit. The problem of the two-frequency irradiation is even more difficult because the Hamiltonian is essentially time-dependent and, therefore, the simulation would require very large number of time steps. It would further decrease the number of spins which can be used in the simulations.

To see whether P_d follows the bi-exponential build-up, as predicted by the kinetic equations Eqs. (3) and (4) (or Eqs. (6) and (7)), cosine pulses with the modulation frequency of 5 kHz and different durations from 200 μs to 50 ms were applied to the thermal equilibrium state, and were followed by the ARRF pulse to monitor P_d. The center frequencies of the pulses were varied from -10 kHz to 10 kHz with a step of 2 kHz. The results are shown in Fig. 3, in which the bi-exponential build-up behavior of P_d is clearly observed.

IV. DISCUSSION

The eigenvalues $\lambda_\pm$ in Eqs. (5) or (10) determine how fast the Zeeman and dipolar polarizations P_S and P_d decay to zero or reach the steady states, and smaller eigenvalues (large absolute values) are favored for faster saturation. From Eq. (5), one can see that λ_- will be smaller when the terms in the square root are smaller. There are two cases when the expressions for the eigenvalues become simple: if $\Delta = -\Delta' = \omega_{\rm loc}$, the two eigenvalues become $-2W$ and $-2W'$. On the other hand, if $W\Delta + W'\Delta' = 0$, the two eigenvalues become $-(W + W')$ and $-(W\Delta^2 + W'\Delta'^2)/\omega_{\rm loc}^2$. For both cases, larger W and W' make the eigenvalues smaller and saturation faster. To obtain a general idea of how the performance of the two-frequency saturation depends on the parameters W, W', Δ, Δ', and $\omega_{\rm loc}$, three numerical calculations were performed, using Eqs. (10).

In the first, Δ and Δ' are fixed, and $\lambda_\pm$ are calculated for varying W and W'. In Fig. 4, the results are shown for $\Delta = 0.5\,\omega_{\rm loc}$ and $\Delta' = -0.3\,\omega_{\rm loc}$, which are randomly chosen to avoid the two special cases discussed above. While λ_+ simply gets smaller as either of W and W' increases, λ_- gets smaller when both of W and W' are larger, most efficiently following the line $W\Delta + W'\Delta' = 0$. So W and W' are supposed to be larger for faster saturation.

In the second, W and W' are fixed and the dependence of $\lambda_\pm$ on Δ and Δ' is investigated. The frequency offsets Δ and Δ' are conveniently represented in units of $\omega_{\rm loc}$. The result when $W = 2W' = 100\,\pi$ is presented in Fig. 5. The two

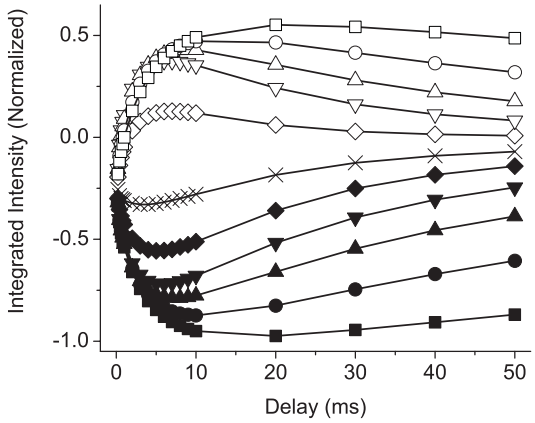

FIG. 3. Time-dependence of the dipolar order. A cosine pulse with modulation frequency 5 kHz was used as the two-frequency pulse. The center frequencies of the cosine pulse were 0 kHz (cross), ±2 kHz (diamond), ±4 kHz (down triangle), ±6 kHz (up triangle), ±8 kHz (circle), and ±10 kHz (square). Open and filled symbols represent the positive and negative frequency offsets, respectively.

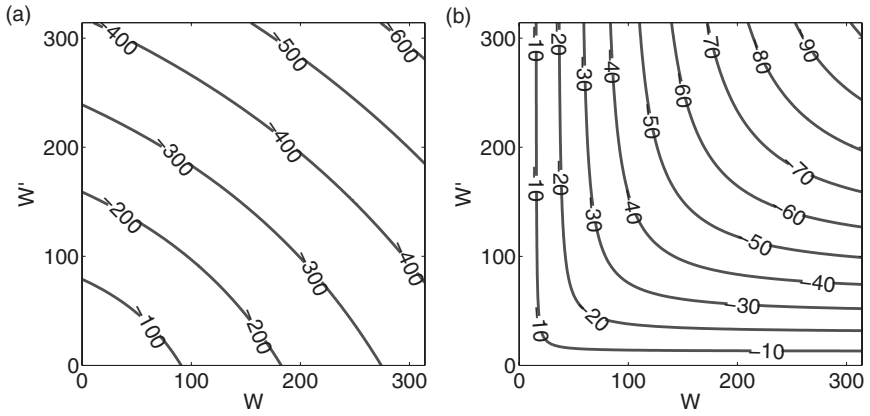

FIG. 4. Eigenvalues (a) λ_+ and (b) λ_- as a function of W and W' when $\Delta = 0.5\,\omega_{\rm loc}$ and $\Delta' = -0.3\,\omega_{\rm loc}$. $T_1 = 1$ s and $T_d = 0.4$ s.

eigenvalues have quite different behavior: λ_+ seems to follow an elliptic paraboloid with its maximum point around the origin, and λ_- appears to decrease quickly along the line $W\Delta + W'\Delta' = 0$. Therefore, it seems that $W\Delta + W'\Delta' = 0$ is a good condition for efficient two-frequency saturation. Since W and W' are positive, it would be beneficial for faster saturation to choose two irradiation frequencies located at opposite sides of the spectrum and farther from the resonance frequency in order to minimize $\lambda_\pm$.

Finally, the dependence of $\lambda_\pm$ on $\omega_{\rm loc}$ has been examined. As an illustration, Fig. 6 shows the result when $W = W' = 100\,\pi$ and $\Delta = -2\Delta'$, which avoids the condition $W\Delta + W'\Delta' = 0$ and shows more general behavior of the eigenvalues: λ_+ quickly increases when $\omega_{\rm loc}$ is very small and becomes constant when $\omega_{\rm loc} > 0.01\Delta$, while λ_- makes a transition from a small value to a value close to zero when $\omega_{\rm loc}$ crosses Δ. Note that $\omega_{\rm loc}$ is a measure of the spectral width. Since the absorption line shape g will be very small when $|\Delta|$, $|\Delta'| \gg \omega_{\rm loc}$, which makes W and W' very small, the huge change of λ_+ shown in Fig. 6 is not practically relevant. If such a regime is excluded, the result shown in Fig. 6 suggests that λ_+ would not significantly depend on $\omega_{\rm loc}$ in the practical regime and that the minimum of λ_- can be searched around $|\Delta| \sim \omega_{\rm loc}$.

In summary, for faster saturation, it is useful to increase W and W' by using a larger rf amplitude and/or choosing the frequency positions of rf irradiation where the absorption line shape g is larger. In addition, it has been found that the saturation can be more efficient when the two irradiation frequencies are located at opposite sides of the resonance frequency, and when the condition $W\Delta + W'\Delta' = 0$ is met. Selecting the frequency positions far from the resonance frequency seems beneficial, but there is a limitation on how large the offsets can be. Normally, g decays fast beyond $\omega_{\rm loc}$, which makes it practically reasonable to make $|\Delta|$ and $|\Delta'|$ comparable to $\omega_{\rm loc}$. In addition, Provotorov's thermodynamic theory assumes $\omega_1 \ll \omega_{\rm loc}$, so a larger $\omega_{\rm loc}$ can allow larger ω_1, thereby making the saturation faster.

In the liquid crystal 5CB, there are two groups of protons, aliphatic and aromatic. Proton spins within a group are strongly coupled by dipole-dipole interactions, while interactions between the spins from different groups are much weaker. As a result, total equilibration and reaching a uniform dipolar temperature is relatively slow. This is the major reason for some deviations between the theoretical and experimental results, as seen in Fig. 2.

The thermodynamic description with two spin temperatures suggests that two irradiation frequencies are needed for fast and uniform saturation. In systems where the quasi-equilibrium state is described by more than two spin temperatures, it would be beneficial to increase the number of

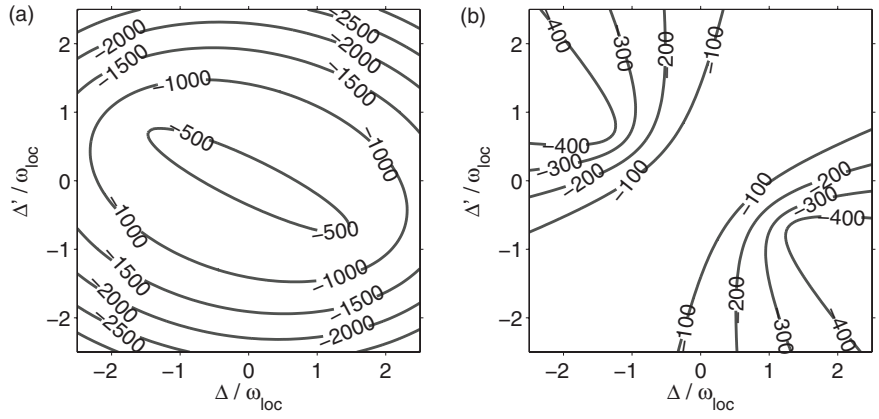

FIG. 5. Eigenvalues (a) λ_+ and (b) λ_- as a function of $\Delta/\omega_{\rm loc}$ and $\Delta'/\omega_{\rm loc}$ when $W = 2W' = 100\,\pi$. $T_1 = 1$ s and $T_d = 0.4$ s.

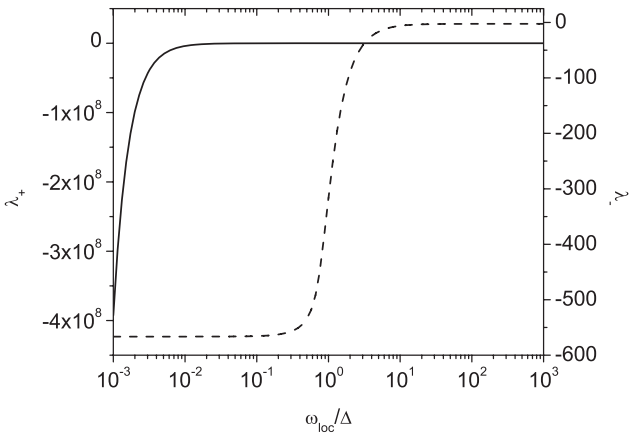

FIG. 6. Eigenvalues λ_+ (solid) and λ_- (dashed) as a function of $\omega_{\rm loc}$ when $\Delta = -2\Delta'$ and $W = W' = 100\,\pi$. $T_1 = 1$ s and $T_d = 0.4$ s.

irradiation frequencies to match the number of independent spin temperatures.

In our experiments, we used cosine-modulated pulses to irradiate symmetrically on two sides of the rf frequency. In some cases, the method may be more conveniently implemented by using a square-shaped modulation. Such modulation is produced by a sequence of two pulses with equal width τ and opposite phases. The Fourier components with the lowest frequencies $\pm\pi/\tau$ would act exactly like the two frequencies of the cosine modulation. The components with higher frequencies have small amplitude and produce insignificant effects.

V. CONCLUSION

We have demonstrated that two-frequency irradiation can be a convenient simple method for fast uniform saturation of spin systems with dipolar couplings. The method is very robust and does not require tuning of the experimental parameters. The theoretical description is based on the application of Provotorov theory, which provides a quantitative description of the experimental results. A liquid-crystalline test system has been used to study different saturation regimes, and it is found that saturation works best in the case where the two irradiation frequencies are placed at opposite sides of the average Larmor frequency. The actual irradiation frequencies are not important as long as there is appreciable spectral density of the dipolar coupled spectrum in this region. The two-frequency irradiation can be used in solid-state and liquid-crystalline NMR for eliminating unwanted signals from a system of strongly coupled spins. In MRI applications, this technique can be utilized for suppressing broad spectral components, saturation in CEST experiments, discrimination between CEST and MT mechanisms, and for improving MRI contrast.

ACKNOWLEDGMENTS

We acknowledge funding from the (U.S.) National Science Foundation (NSF) under Grant No. CHE0957586, and from the National Institutes of Health (NIH) under Grant No. R21AR055724.

[1] R. R. Ernst, G. Bodenhausen, and A. Wokaun, *Principles of Nuclear Magnetic Resonance in One and Two Dimensions* (Clarendon, Oxford, 1988).
[2] A. Abragam, *Principles of Nuclear Magnetism* (Oxford University Press, Oxford, 1961).
[3] M. Goldman, *Spin Temperature and Nuclear Magnetic Resonance in Solids* (Clarendon, Oxford, 1970).
[4] C. P. Slichter, *Principles of Magnetic Resonance*, 3rd ed. (Springer, Berlin, 1996).
[5] J. Zhou and P. C. M. van Zijl, Prog. Nucl. Magn. Reson. Spectrosc. **48**, 109 (2006).
[6] R. M. Henkelman, G. J. Stanisz, and S. J. Graham, NMR Biomed. **14**, 57 (2001).
[7] N. Tjandra and A. Bax, Science **278**, 1111 (1997).
[8] J. W. Emsley and J. C. Lindon, *NMR Spectroscopy Using Liquid Crystal Solvents* (Pergamon, New York, 1975).
[9] J.-S. Lee and A. K. Khitrin, J. Chem. Phys. **122**, 041101 (2005).
[10] B. N. Provotorov, Zh. Eksp. Teor. Fiz. **41**, 1582 (1961).
[11] J.-S. Lee and A. K. Khitrin, J. Chem. Phys. **128**, 114504 (2008).